Electronic Supplementary Material (ESI) for Physical Chemistry Chemical Physics.

Supporting Information

Room-Temperature Ferromagnetism and Exchange Bias in Chromia Core-Shell Nanoparticles Containing a Nickel(II)-Chromia Shell: Experiment and First Principles Calculations

Authors: M. D. Hossain[1], R. A. Mayanovic[1*], S. Dey[1†], R. Sakidja[1], M. Benamara[2]

Affiliations:

[1]Department of Physics, Astronomy & Materials Science, Missouri State University, Springfield, MO 65897.

[2]University of Arkansas Nano-Bio Materials Characterization Facility, University of Arkansas, Fayeteville, AR 72701, USA.

*robertmayanovic@missouristate.edu.

†Current address: 1420 Sand Creek Road, Albany, NY 12205.

Experimental

Scanning Electron Microscopy

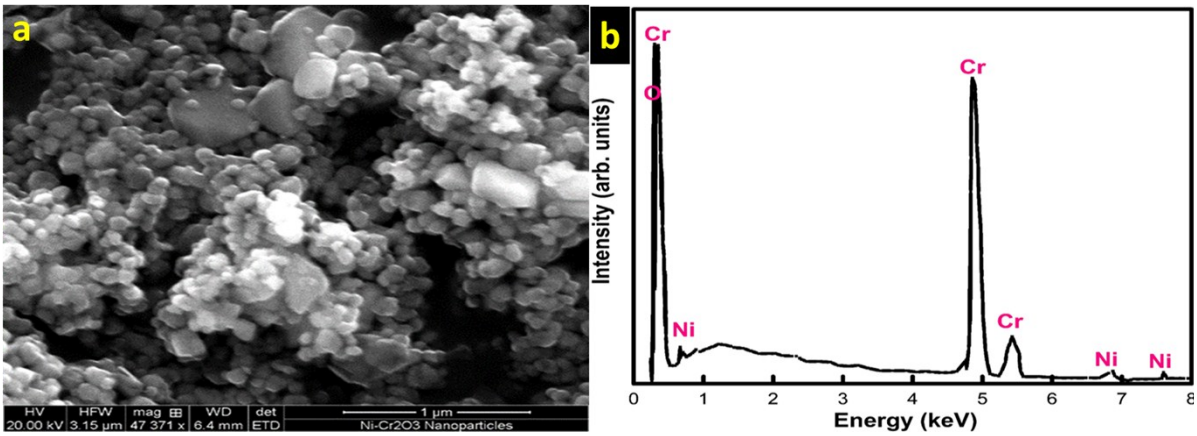

Fig. S1 (a) An SEM image showing that most of the nanoparticles are spherical in shape and are agglomerated. (b) SEM-EDX data confirms the presence of Ni, Cr and O in the nanoparticles.

Transmission Electron Microscopy

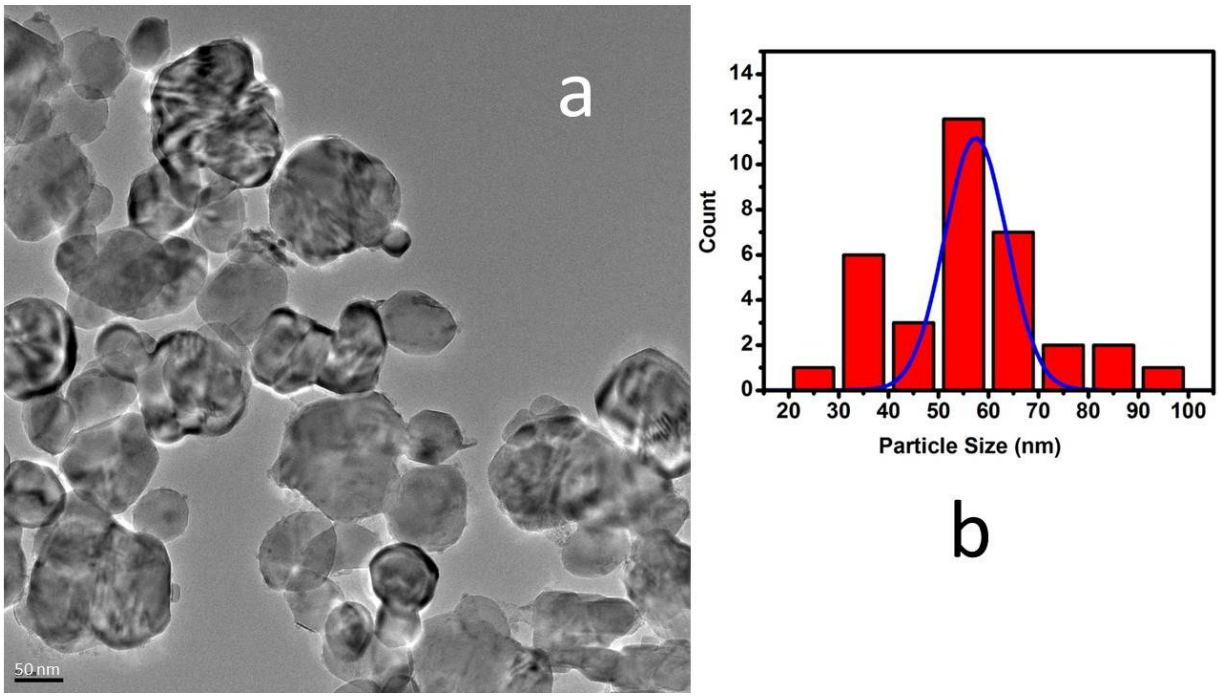

Fig. S2 a) TEM image of several CSNs used to estimate their mean size and b) a histogram plot of the size distribution of the CSNs and the Gaussian fit (blue line) to the distribution.

Rietveld Refinement of the XRD Data

The amorphous like background in the XRD pattern is due to the glass substrate used to hold the CSN sample. The incident beam profile and peak asymmetry of the diffractometer were modeled using fundamental peak function[5] from a CeO_2 standard (NIST 674b) XRD data.[6] The lattice parameters of the corundum unit cell, z-position of the Cr atom, x-position of the O atom were refined for the α-Cr_2O_3 core and α-$Ni_{0.58}Cr_{1.42}O_{2.88}$ shell of CSNs. For the shell region, Cr, Ni and O (to account for oxygen vacancy formation) atoms with partial site occupancies were used in the atomic sites within the refinement. The partial site occupancies (in summation form for Cr and Ni), lattice parameters, and Debye-Waller factors were constrained relative to the values used for refining the structure of the α-Cr_2O_3 core. The structural parameters from the refinement are given in the Table S1 shown below.

Table S1. Summary of structural results obtained from Rietveld refinement for α-Cr_2O_3@α-$Ni_{0.58}Cr_{1.42}O_{2.88}$ CSNs.

Core: α-Cr_2O_3 (SG #167: $R\bar{3}c$); a = b = 4.95160(23) Å; c = 13.57448(80) Å ; V = 288.233(32) Å^3; core size = 47.7(16) nm					
Atoms	x	y	z	Site occupancy	B (Å^2)
Cr	0	0	0.34751(29)	1.0	0.6
O	0.3291(26)	0	1/4	1.0	0.6
Shell: α-$Ni_{0.58}Cr_{1.42}O_{2.88}$ (SG #167: $R\bar{3}c$); a = b = 4.96318(17) Å; c = 13.60696(57) Å ; V = 290.276(24) Å^3; core-shell size = 57.3(29) nm					
Ni	0	0	0.347(35)	0.29	0.6
Cr	0	0	0.34(15)	0.71	0.6
O	0.3097(18)	0	1/4	0.96	0.6
Impurity phase: NiO (SG Fm-3m); a= 4.0873(27) Å					
Ni	0	0	0	1	0.414
O	1/2	1/2	1/2	1	0.61

X-Ray Photoemission Spectroscopy

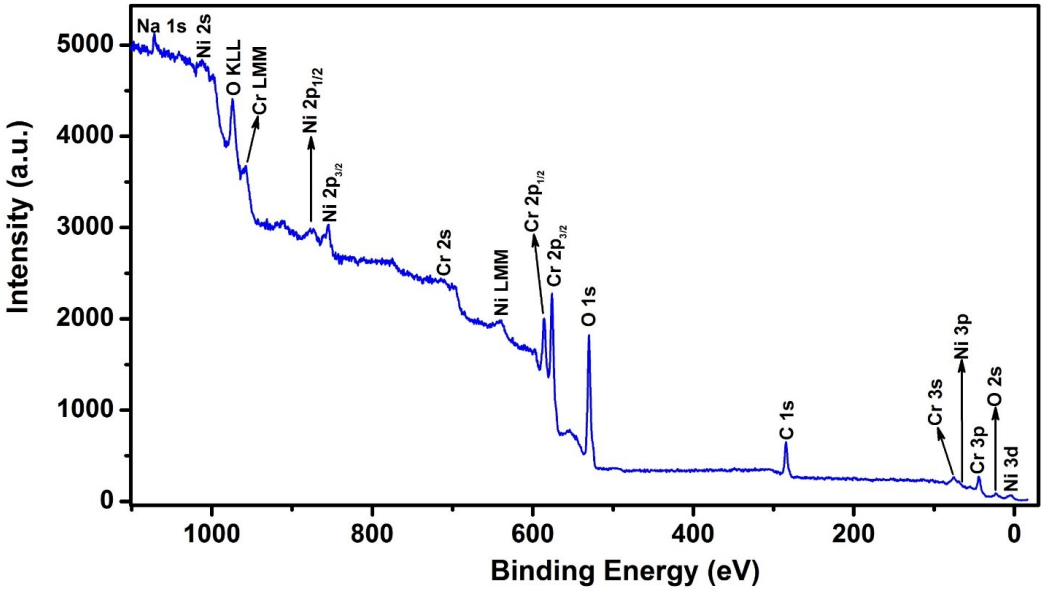

Fig. S3 XPS survey scan of α-Cr_2O_3@α-$Ni_{0.58}Cr_{1.42}O_{2.88}$ CSNs. The C originates predominantly from the carbon tape containing the sample.

Table S2. Results from fitting of the high-resolution XPS spectra measured from the CSNs. GL(30) indicates a Gaussian-Lorentzian product formula where the percentage of Lorentzian peak shape is indicated in the parenthesis.

$Cr2p_{3/2}$		**Position**	**FWHM**	**Line Shape**	**Area**	**%Area**
Cr-O	Peak-1	573.37	2	GL(30)	421.11	11.63
	Peak-2	574.61	1.6	GL(30)	421.11	11.63
	Peak-3	575.68	2	GL(30)	1684.42	46.51
	Peak-4	577.53	2	GL(30)	421.11	11.63
Cr-OH		576.8	1.8	GL(30)	673.77	18.68
O1s						
Cr-O		528.8	3.1	GL(30)	2800	59.92
Ni-O		529.68	1.34	GL(30)	280	5.95
Cr-OH		530.1	2.8	GL(30)	1484	31.55
Ni-OH		532.22	1.64	GL(30)	140	2.98
$Ni2p_{3/2}$						
Ni-O		853.42	5.18	GL(30)	1242.23	51.24
Ni-OH		854.95	3	GL(30)	372.67	15.37
Satellite		859.91	5.5	GL(30)	809.24	33.38

Table S3. Elemental analysis from XPS data measured from the α-Cr_2O_3@α-$Ni_{0.58}Cr_{1.42}O_{2.88}$ inverted core-shell NPs. The analysis for elemental content using the $Cr2p_{3/2}$, O1s and $Ni2p_{3/2}$ peaks was accomplished using a Shirley background.

Element	**Peaks**	**Position**	**FWHM**	**Area**	**Atomic %**
Cr	$Cr2p_{3/2}$	576.23	3.7	4870	26.17
O	O1s	530.23	3.5	4769.02	68.47
Ni	$Ni2p_{3/2}$	854.73	4.9	2068.9	5.35

Ni Concentration Estimation in α-Cr_2O_3@α-$Ni_xCr_{2-x}O_y$ Core-Shell Nanoparticles

The average particle size determined using XRD and TEM is 57 nm and HRTEM shows a shell thickness of 5 nm. Considering an XPS sample depth of 10 nm, the outer radius R=28.5 nm, the radius of the core is r_2=23.5 nm and the radius to the penetration depth is r_1=18.5 nm as shown in Fig. S11. The volume ratio of the shell vs XPS sampling volume z = 0.6,

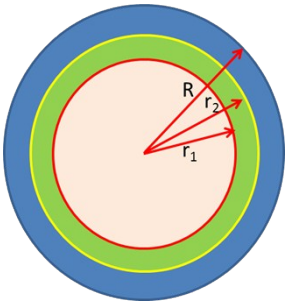

Fig. S4. Schematic of a core-shell nanoparticle with dimensions as outlined in the text. We assume a 10 nm sampling depth of XPS.

The atomic percentages calculation from XPS survey scan provides Ni:Cr:(O+OH) = 5.35 : 26.17 : 68.47; excluding the OH contribution Ni:Cr:O= 5.35 : 26.17 : 44.62 and normalization gives final atomic percentages of Ni:Cr:O= 7.03 : 34.37 : 58.6.

For determining the concentration x value in the sample we will use the sampling volume in the formula of $(1-z)\bullet[Cr_2O_3] + z\bullet[Ni_xCr_{(2-x)}O_p]$;

$0.0703Ni + 0.3437Cr + 0.586O = 0.4\bullet[0.4Cr + 0.6O] + 0.6\bullet[yNi + (0.423-y)Cr + 0.577O]$

This gives y=0.1167 and x=5*0.1167 ≈ 0.58, the corresponding value of p for O, p=2.88. Thus the final formula for the shell is $Ni_{0.58}Cr_{1.42}O_{2.88}$

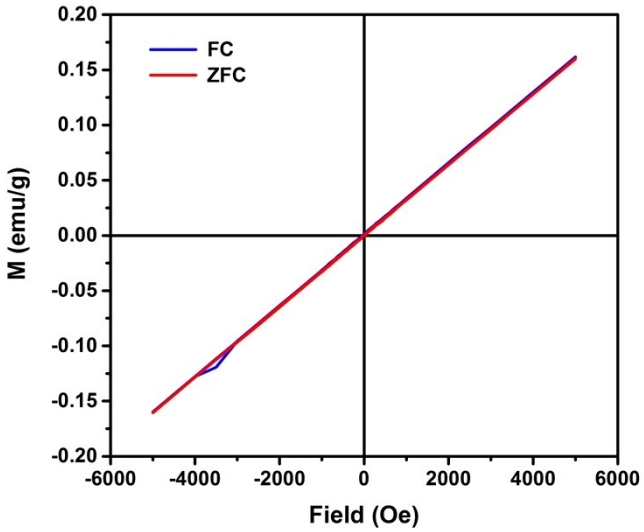

Fig. S5. Magnetization hysteresis curves measured from α-Cr_2O_3 NPs at 300 K in the zero field cooled (ZFC) and field cooled (FC) condition at 20 kOe.

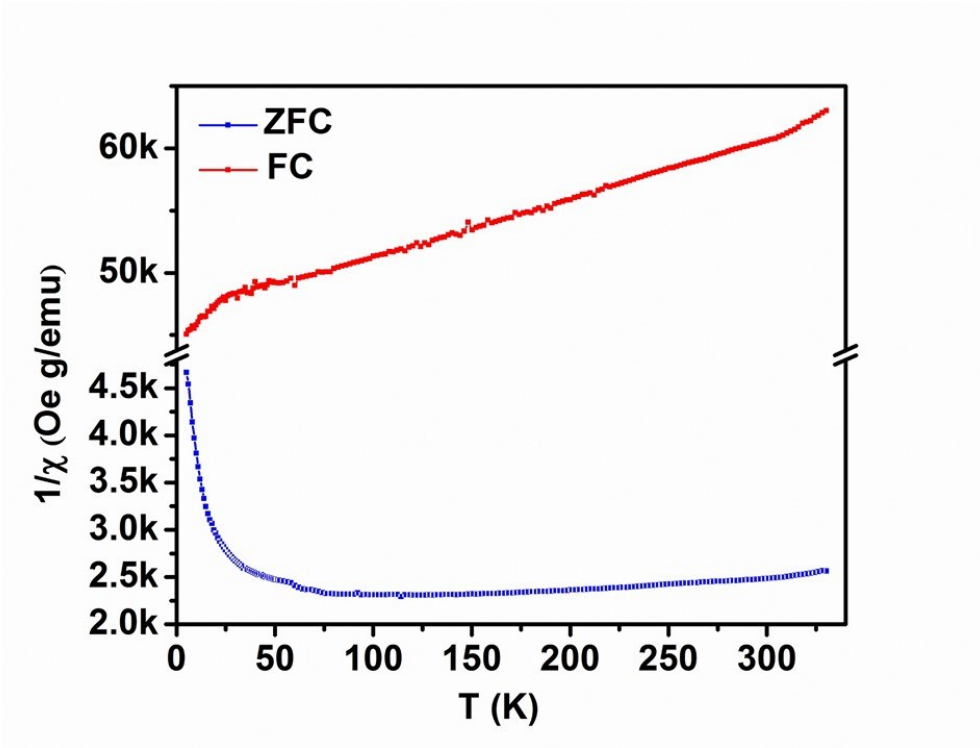

Fig. S6. Inverse susceptibility (1/χ) curves measured from our α-Cr_2O_3@α-$Ni_{0.58}Cr_{1.42}O_{2.88}$ CSNs in the ZFC and FC condition as a function of temperature. Note that the magnitude of 1/χ is given in engineering notation, e.g., 2.0k is equal to 2000 Oe·g/emu.

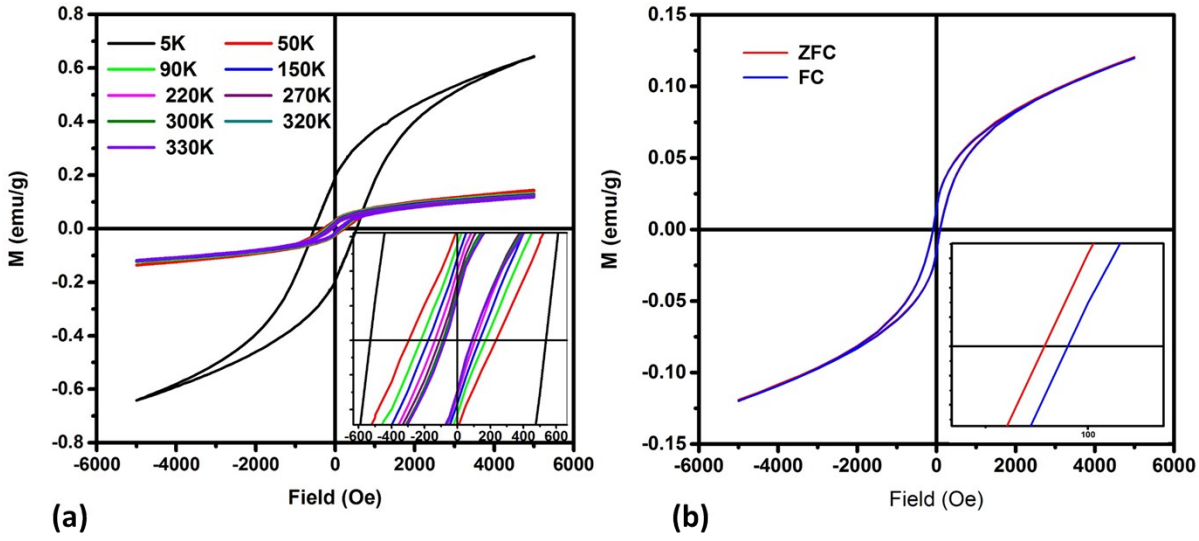

Fig. S7. (a) Magnetization hysteresis curves measured from α-Cr_2O_3@α-$Ni_{0.58}Cr_{1.42}O_{2.88}$ CSNs in the ZFC condition at different temperatures: The inset shows an enlarged view of the data at the

origin. (b) The FC and ZFC magnetization hysteresis measured at 300 K: The inset shows the shift between the FC and ZFC hysteresis curves at the M = 0 value.

UV-Vis Measurements

A suspension of the CSNs was made in DI water and allowed to evaporate on a microscope glass slide. An Ocean Optics HR 4000 spectrophotometer and a fiber-optic coupled DT-Mini-2 deuterium/tungsten-halogen lamp source (Ocean Optics) were used to measure the UV-Vis transmission/absorption spectra of the CSNs. The accumulated spectra were collected in ~160 ms. The energy band gap value ~2.5(1) eV of the CSNs was estimated from the intersection of the fitted line of function $(\alpha \cdot h\nu)^{1/2}$, where α is the absorption coefficient, at the zero point with the energy ($h\nu$) axis as shown in Fig S5. Using similar analysis of UV-Vis spectra measured from our α-Cr_2O_3, we obtain a band gap value of ~3.0(1) eV.

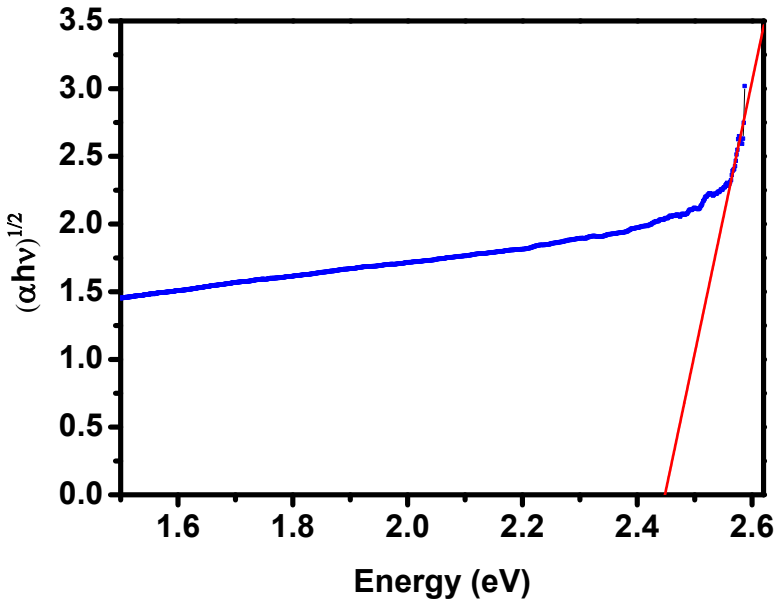

Fig. S8. The $(\alpha \cdot h\nu)^{1/2}$ quantitity plotted vs photon energy ($h\nu$) as determined from the UV-Vis absorption spectra measured from the CSNs. The extrapolated fitted line intersects the energy axis at 2.45 eV.

Computational Details

The calculation of partial charges on Ni, Cr and O atoms was made using Bader's procedures, which provides accurate atomic charges for plane wave basis functions, and a program that employs a fast algorithm for performing the Bader analysis.[7] The Bader charge analysis of the α-Cr_2O_3 and α-Ni(II)Cr_3O_6 structures is shown in Table S4. Electron localization function (ELF)

analysis was performed using procedures described elsewhere;[8,9] the ELF images were generated using the visualization software Vesta.[10]

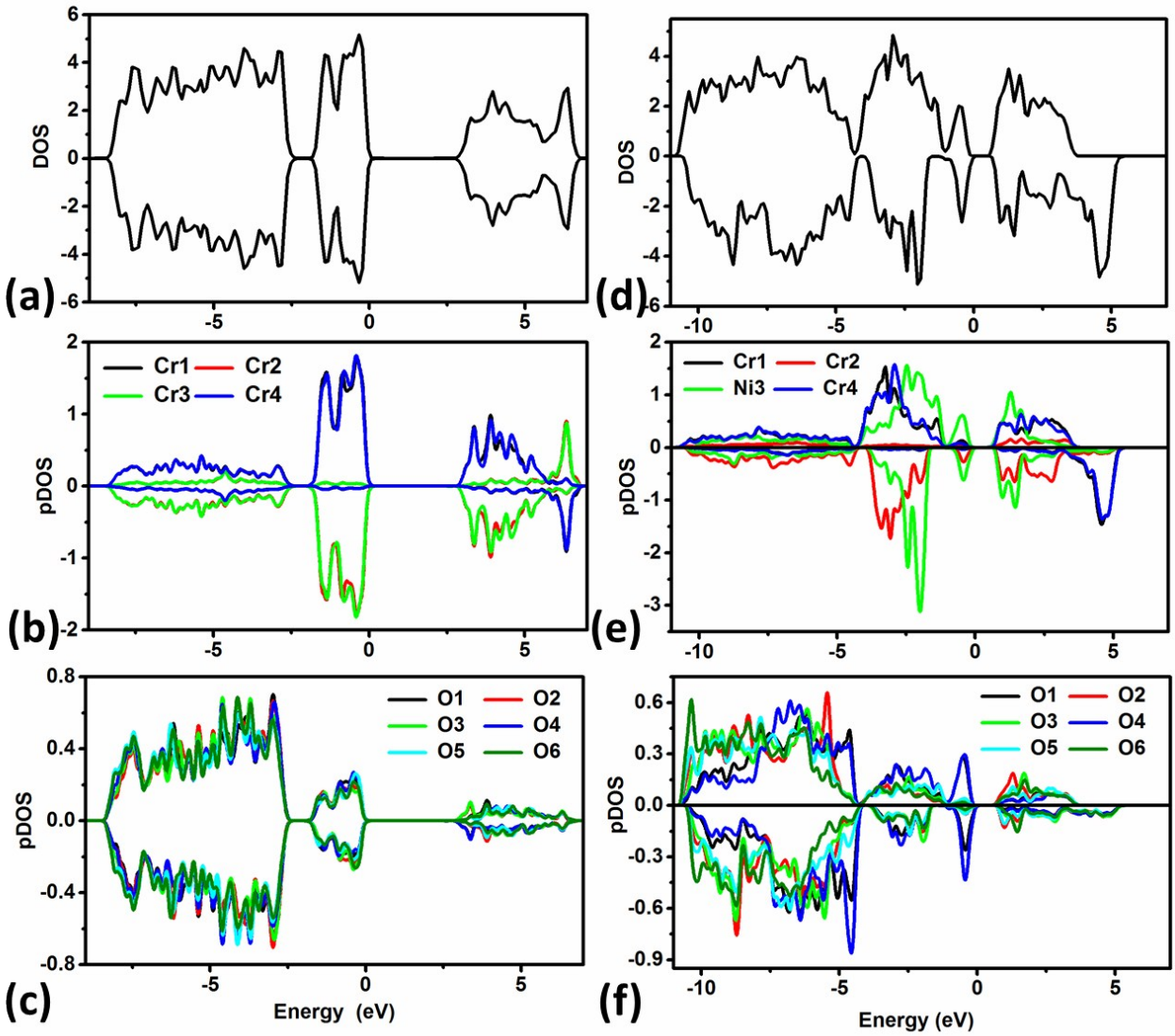

Fig. S9. DFT-based calculation results as follows: α-Cr_2O_3 structure (a) DOS (b) pDOS of Cr 3d orbital (c) pDOS of O 2p orbitals; α-Ni(II)Cr_3O_6 structure (d) DOS (e) pDOS of Cr and Ni 3d orbital (f) pDOS of O 2p orbitals.

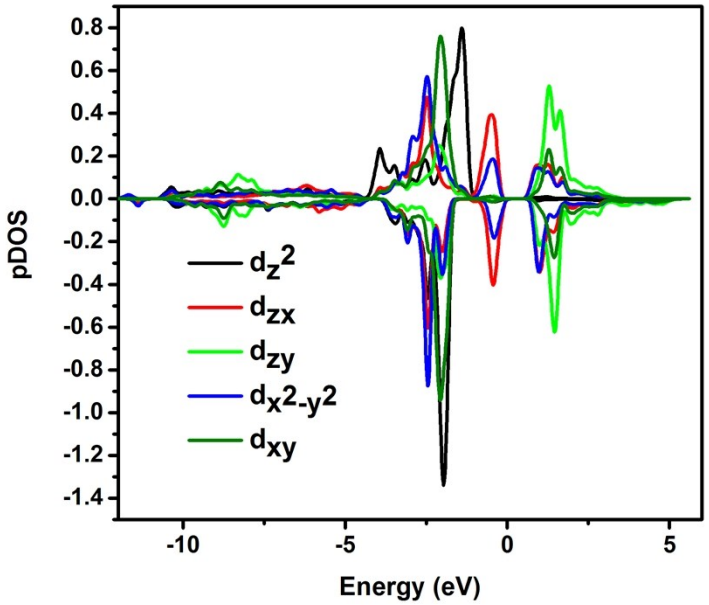

Fig. S10. The pDOS plot showing the Ni(II) t_{2g} (d_{xy}, $d_{zx,}$ d_{zy}) and e_g (d_z^2 & d_x^2-$_y^2$) orbitals of α-Ni(II)Cr_3O_6.

Table S4: Computed magnetic moments of individual atoms in α-Cr_2O_3 and α-Ni(II)Cr_3O_6.

Atom	α-Cr_2O_3 (in μ_B)	α-Ni(II)Cr_3O_6 (in μ_B)
Cr1	+3.11	+3.12
Cr2	-3.11	-3.10
Cr3/Ni	-3.11	+0.12
Cr4	+3.11	+3.09

Table S5: Bader partial charge analysis of α-Cr_2O_3 and α-Ni(II)Cr_3O_6 in the primitive rhombohedral 1x1x1 structures; e is the fundamental charge unit of ~1.6 x 10^{-19} C.

Atom	**Charge (α-Cr_2O_3) ·e**	**Charge (α-Ni (II)Cr_3O_6) ·e**
O1	-1.6761	-1.5665
O2	-1.676	-1.4373
O3	-1.6925	-1.4264
O4	-1.6923	-1.6156

O5	-1.7137	-1.502
O6	-1.7139	-1.5014
Cr1	+2.5409	+2.5191
Cr2	+2.5409	+2.4707
Cr3/Ni3	+2.5412	+0.5468
Cr4	+2.5412	+2.5121

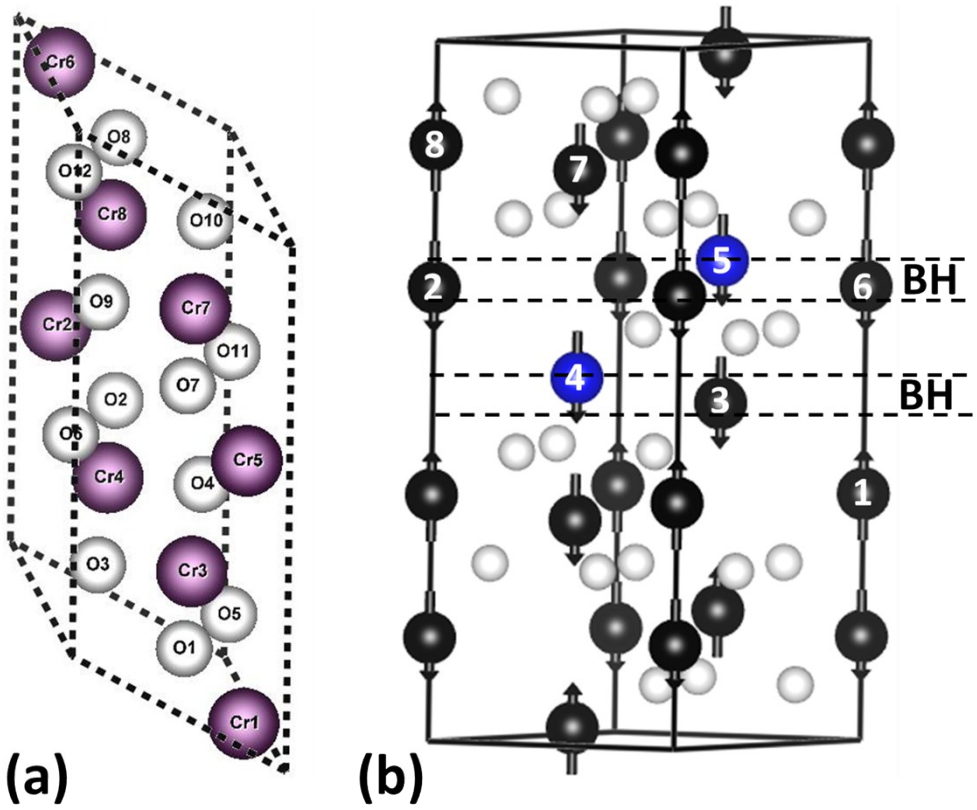

Figure S11: a) A diagram of the 20 atom 1x1x2 supercell showing the Cr and O atomic positions; in the first principles calculations, two Ni atoms are substituted. b) A 30 atom unit cell with the 8 cation positions marked in accordance to the 1x1x2 supercell. The final spin configurations are shown in the buckled honeycomb (BH) plane for Ni4-Ni5 (Case-5) substitution. The substitutional Ni spins are aligned with the surrounding tri-cluster Cr spins in the BH planes whereas the remainder of the structure maintains the original AFM configuration. The arrows representing the magnetic moments on the cations are not drawn to scale.

Table S6 shows the results from our DFT-based calculations for the energy values relative to the two nearest substituted Ni's in the supercell and the overall magnetic moment of the α-$Ni_2(II)Cr_6O_{12}$ structure, for the cases of substitutional positions described below. Cases 1 correspond to having two nearby ++ Ni's (Fig. S9 a) and b)) substituted in the BH plane of the corundum structure; cases 2 represents substitution in the same BH plane; cases 3 and 4 correspond to substitution in alternate BH planes. Case 5 is substitution in adjoining BH planes. Cases 6 is the substitution in the alternate BH planes and farthest apart from each having opposite spin configuration. The relative energy values are calculated with respect to the Case-3.

Table S6: Calculation results for substitution of two Ni atoms for Cr atoms in various sites in a 20 atom 1x1x2 supercell.

	Substitution Sites	Initial Spin Configuration	Final Spin Configuration	Energy difference (eV)	Overall Magnetic Moment (μ_B)
Case-1	3-5	-+	-+	0	0
Case-2	3-4	-+	-+	-0.01	0
Case-3	4-7	+-	+-	+0.17	0
Case-4	3-8	-+	-+	+0.17	0
Case-5	4-5	++	--	+0.10	-5.92
Case-6	4-1	++	--	+0.16	-4.03

References

(1) Schneider, C. A.; Rasband, W. S.; Eliceiri, K. W. *Nat. Methods* **2012**, *9* (7), 671–675.
(2) Cheary, R. W.; Coelho, A. *J. Appl. Crystallogr.* **1992**, *25* (2), 109–121.
(3) Coelho, A. A. *J. Appl. Crystallogr.* **2003**, *36* (1), 86–95.
(4) Balzar, D.; Audebrand, N.; Daymond, M. R.; Fitch, A.; Hewat, A.; Langford, J. I.; Le Bail, A.; Louër, D.; Masson, O.; McCowan, C. N.; Popa, N. C.; Stephens, P. W.; Toby, B. H. *J. Appl. Crystallogr.* **2004**, *37* (6), 911–924.
(5) Thompson, P.; Cox, D. E.; Hastings, J. B. *J. Appl. Crystallogr.* **1987**, *20* (2), 79–83.
(6) Finger, L. W.; Cox, D. E.; Jephcoat, A. P. *J. Appl. Crystallogr.* **1994**, *27* (6), 892–900.
(7) Henkelman, G.; Arnaldsson, A.; Jónsson, H. *Comput. Mater. Sci.* **2006**, *36* (3), 354–360.
(8) Silvi, B.; Savin, A. *Nature* **1994**, *371* (6499), 683–686.
(9) A. D. Becke, K. E. J. E. *J. Chem. Phys.* **1990**, *92* (9), 5397–5403.
(10) Momma, K.; Izumi, F. *J. Appl. Crystallogr.* **2011**, *44* (6), 1272–1276.